Cherenkov diffraction radiation dielectric button characterization via a slab-line

C Pakuza[1] **and M Wendt**[2]

[1] John Adams Institute for Accelerator Science, University of Oxford, Oxford, UK
[2] CERN, Geneva, Switzerland

E-mail: `collette.pakuza@physics.ox.ac.uk, manfred.wendt@cern.ch`

Abstract. *Cherenkov* diffraction radiation is generated when a charged particle beam passes in close proximity to a dielectric target, and is currently being studied and developed for various non-invasive beam instrumentation applications at CERN. One such instrument is a beam position monitor (BPM) composed of four cylindrical dielectric inserts. A challenge of using the conventional stretched wire technique to characterize the BPM up to high frequencies is the coupling of unwanted higher order modes (HOM) into the inserts that are dielectric-loaded circular waveguides. To minimize the generation of HOMs and excite mainly the transverse electromagnetic (TEM) mode as a model of the beam field, a set-up comprising a dielectric insert mounted on a slab line with 50 Ω characteristic impedance was tested. The results and comparison with numerical simulations in CST are be presented.

1. Introduction

The *Advanced Proton Driven Plasma Wakefield Experiment* (AWAKE) at CERN is a proof-of-principle plasma acceleration experiment that uses high intensity proton bunches to generate high-gradient accelerating wakefields of ∼1 GeV/m in a cell of rubidium vapor, which is ionized by a laser pulse, to accelerate an electron bunch to high energies [1]. The monitoring of the transverse position of the co-propagating proton and electron beam bunches near the plasma cell is essential to overlap the proton and electron beam trajectories, but appears to be particularly challenging as both beam bunches pass the BPM pickup location – within a few 10 ps . However, the proton and electron bunch parameters are different. The non-*Gaussian* p-bunch has a RMS bunch length of 6 - 8 cm and $(2.5 - 3.1) \times 10^{11}$ charges per bunch, while the e^- RMS bunch length is ∼1.2 mm, has a *Gaussian* particle distribution, and a much lower intensity, $(0.6 - 6.2) \times 10^9$ charges per bunch. While the position measurement of a high intensity proton bunch in the presence of an electron bunch with ∼100 × lower intensity is almost straightforward, the pure, unperturbed monitoring of the electron bunch position in the presence of the high intensity proton bunch turns out to be more difficult.

As of the different signal spectra for the proton and electron bunches, frequency discrimination is viewed as the favorable separation method and can be implemented already at the beam pickup. Therefore, a new detection method based on *Cherenkov* diffraction radiation [2] is under development to pickup only the high frequency content of the electron bunch spectrum, were the proton bunch spectrum is effectively vanished [3, 4]. A *Cherenkov* diffraction radiation beam position monitor (ChDR BPM) operates similar to popular broadband electromagnetic BPM pickups, e.g. button-type or stripline BPMs, and consists out of four electrodes, symmetrically

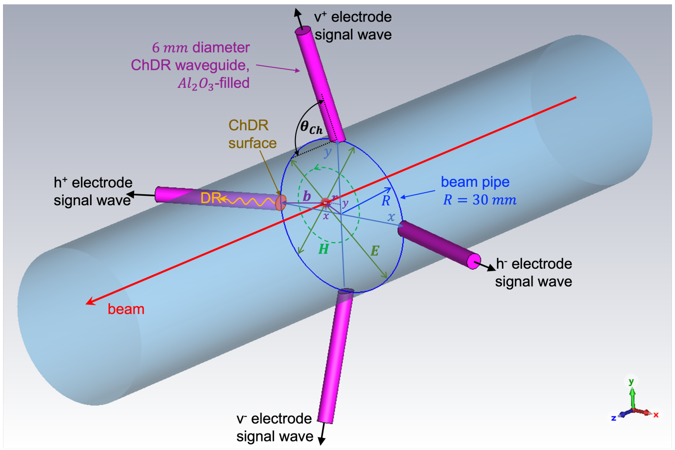

Figure 1: A BPM based on *Cherenkov* diffraction radiation.

arranged in the horizontal and vertical plane. Figure 1 shows a simplified model of the ChDR BPM pickup electrode assembly in the 60 mm diameter vacuum chamber of AWAKE. Each ChDR electrode is an Al_2O_3-ceramic ("alumina") filled circular waveguide of 6 mm diameter, facing the vacuum chamber flush under the *Cherenkov* angle $\theta_{Ch} = \arccos(1/\beta n) \approx 71°$, with $n = \sqrt{\epsilon_r}$ being the refractive index of alumina ($\epsilon_r \approx 9.9$), and for the 16 MeV electron beam energy in AWAKE at a relativistic velocity $\beta = v/c = 0.9995 \approx 1$.

Notably at ≥ 16 MeV energy, the electromagnetic (EM) field of the bunched beam has only transverse components, as illustrated in Fig. 1, a so-called transverse electro-magnetic (TEM) beam field. The beam passes the four ChDR electrodes with some transverse beam offset $\vec{r}(x, y)$, thus the transverse distance between beam and ChDR radiator surface (see also Fig. 1) is $\vec{b} = R - \vec{r}$, and $b = |\vec{b}|$ called the *impact parameter*. *Polarization radiation* is generated by the beam field, as wanted *Cherenkov* diffraction radiation at the surface of the four waveguide radiators, but also as unwanted diffraction radiation from the edges of the waveguides. The EM-field intensity of the polarization radiation generated at each ChDR radiator depends on a variety of parameters

$$EM_{PR} = g(b, \gamma, \lambda, Q, \sigma, \epsilon_r, \phi) \tag{1}$$

with particle energy given by the *Lorentz* factor $\gamma = (1 - \beta^2)^{-1/2}$, the charge Q of the *Gaussian* bunch of length σ, the observation frequency f, which is related to the wavelength $\lambda = c/f$, the permittivity ϵ_r of the ChDR radiator material, and the relative surface area ϕ the radiator covers wrt. the beam pipe surface. The symmetric arrangement of 2+2 identical ChDR radiators as shown in Fig. 1 then allows a *normalization* of the detected ChDR radiator signals, thus a horizontal and vertical position measurement of the bunched beam

$$\text{hor. pos.} \propto \frac{\text{h}^+ - \text{h}^-}{\text{h}^+ + \text{h}^-}, \qquad \text{vert. pos.} \propto \frac{\text{v}^+ - \text{v}^-}{\text{v}^+ + \text{v}^-}.$$

2. The slab-line setup

Beside a few basic properties which can be computed analytically, like the *Cherenkov* angle, most of the design and optimization of the ChDR BPM is realized by using numerical EM simulation software, e.g. *CST Studio*. Between EM simulations and beam measurements in the AWAKE test accelerator, there is a rather large gap in understanding and knowledge of this new type of beam pickup, and a characterization in the laboratory under easy controllable conditions seems valuable. BPMs and other electromagnetic beam pickups are usually characterized with a coaxial measurement setup, with the center conductor emulating the beam field stimulated by a test signal. e.g. from a pulse generator or a RF sweep-generator, as part of a vector network

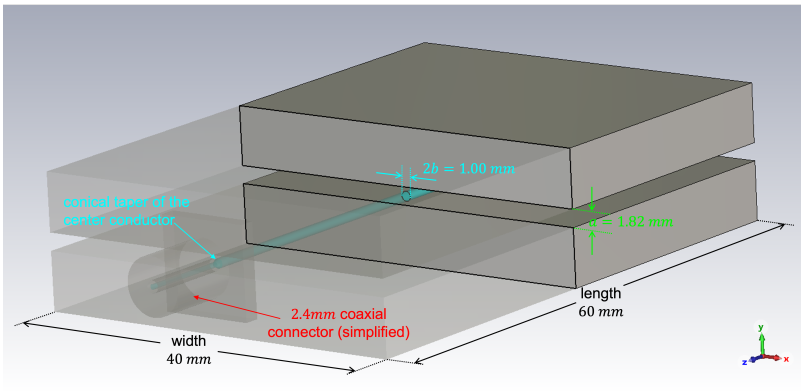

Figure 2: Slabline steup.

analyzer (VNA). Unfortunately non-TEM higher-order modes limit the frequency range of a coaxial setup with $D = 2R = 60\,\text{mm}$ to

$$f_{TE11coax} = \frac{c}{\pi\sqrt{\mu_r \epsilon_r}\left(\frac{D+d}{2}\right)} \lessapprox 3.18\,\text{GHz} \tag{2}$$

assuming air dielectric ($\epsilon_r = 1$, $\mu_r = 1$) and a center conductor of very thin diameter d. A characterization to frequencies up to $\sim 40\,\text{GHz}$ would limit the outer beam pipe diameter to $D \lessapprox 4.8\,\text{mm}$, which is incompatible with the 6 mm diameter size of the ChDR "button" radiator.

A *slab-line* configuration proved to be a suitable broadband test setup to characterize the transfer response of the ChDR radiator in the frequency range DC$-$ 44 GHz. Figure 2 shows the setup schematically, which consists of a cylindrical conductor of diameter $2b = 1.00\,\text{mm}$, symmetrically sandwiched between two ground planes at a distance of $a = 1.82\,\text{mm}$, to achieve a characteristic impedance

$$Z_{SL} = \eta_0 \left[\frac{1}{2\pi} \ln\left(\frac{2a}{\pi b}\right) - \frac{0.2153R^2}{1 + 5.682R^2}\right] \tag{3}$$

of $Z_{SL} = 50\,\Omega$ [5], where $\eta_0 \cong 120\pi\,\Omega$ is the wave impedance in free space and $R = (b/a)^2$. The dimensions of the slab-line setup, length 60 mm and width 40 mm, have been chosen for practical reasons, e.g. to accommodate the ChDR target, no sag of the center conductor, etc., and to have a reasonable low EM-field near the outer perimeter, see also Fig. 3.

Figure 4 shows the characteristic impedance $Z_{SL}(t)$ along the slab-line, including the two 2.4 mm coaxial connectors at both ends, numerically calculated with the *CST Studio* software (dashed traces) and measured with a *Keysight* P5007A USB VNA (solid traces). Therefore, the VNA was operated in *time-domain, TDR step response* mode, i.e., while the VNA measures the $S11(f)$ scattering parameter – the reflection coefficient $\Gamma(f)$, which is the ratio of the reflected and incident voltage waves – in the frequency range 10 MHz – 44 GHz, an inverse fast *Fourier*

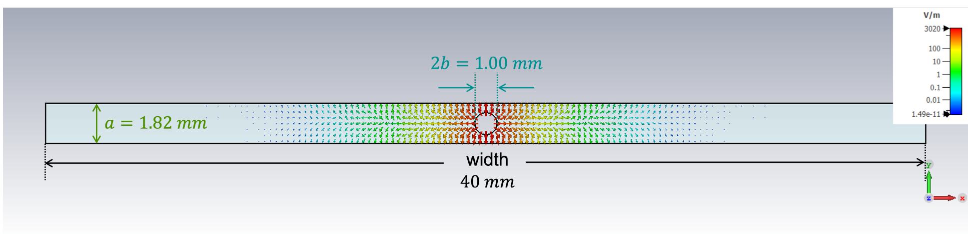

Figure 3: Transverse E-field across the slab-line.

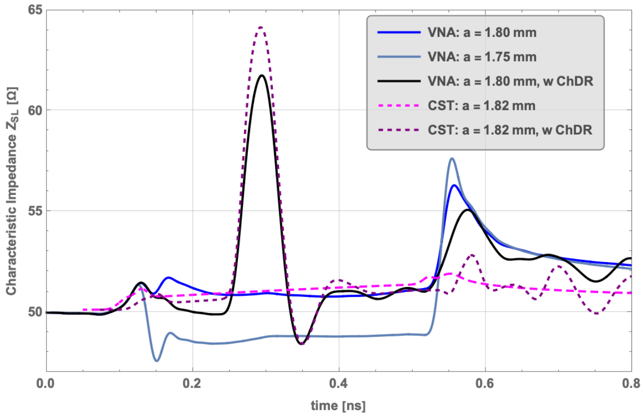

Figure 4: Characteristic impedance Z_{SL} along the slab-line.

transform (iFFT) together with a factor $\delta(f)/2+1/j2\pi f$ (step function in the frequency-domain) is applied to the S11 data, which is equivalent to a *time-domain reflectometry* TDR measurement. The instrument converts the resulting time-domain reflection coefficient $\Gamma(t)$ to the impedance in time-domain

$$Z(t) = Z_0 \frac{1+\Gamma(t)}{1-\Gamma(t)}, \tag{4}$$

where $Z_0 = 50\,\Omega$ is the reference impedance and the time is equivalent to the longitudinal space coordinate, $s = v_p t/2$, with the phase velocity $v_p = c/\sqrt{\varepsilon_r} \cong 2.998 \times 10^8\,\mathrm{m/s}$ because of the air dielectric $\varepsilon_r = 1$. In practice, the transition between the slab-line and the coaxial line (2.4 mm connector) is substantially more inductive (higher characteristic impedance Z_{SL} peaks at $t \approx 150\,\mathrm{ps}$ and $t \approx 550\,\mathrm{ps}$) than the *CST* simulation predicts. Manufacturing tolerances and assembly precision play a major role to control Z_{SL}, a variation in the distance of the two ground planes, $a = 1.75\,\mathrm{mm}$ and $1.80\,\mathrm{mm}$, results in $Z_{SL} \approx 48.5\,\Omega$ and $\sim 51\,\Omega$ respectively.

As of today there exists no analytical modal analysis for non-TEM higher-order modes for the slab-line. Therefore, we carried out a numerical higher-order mode analysis which shows three non-TEM eigenmodes exist for frequencies $< 44\,\mathrm{GHz}$, around 14 GHz, 31 GHz and 42 GHz. However, none of those eigenmodes are excited through the coaxial launchers, also demonstrated by a numerical analysis and verified by a measurement of the $S21$ transmission function between the two coaxial connectors with the VNA.

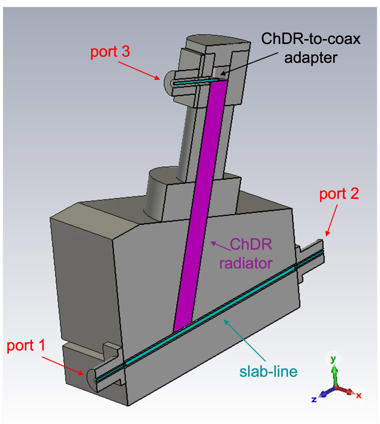

(a) Physical model with coaxial adapter.

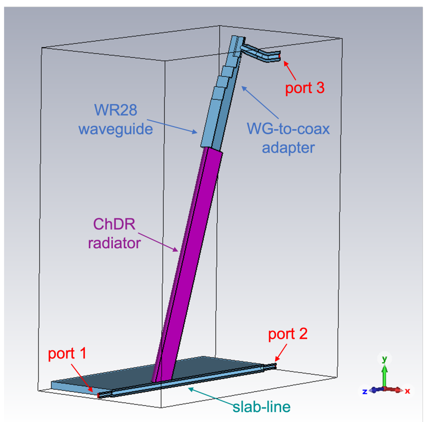

(b) ChDR radiator slabline setup.

Figure 5: ChDR radiator slabline setup.

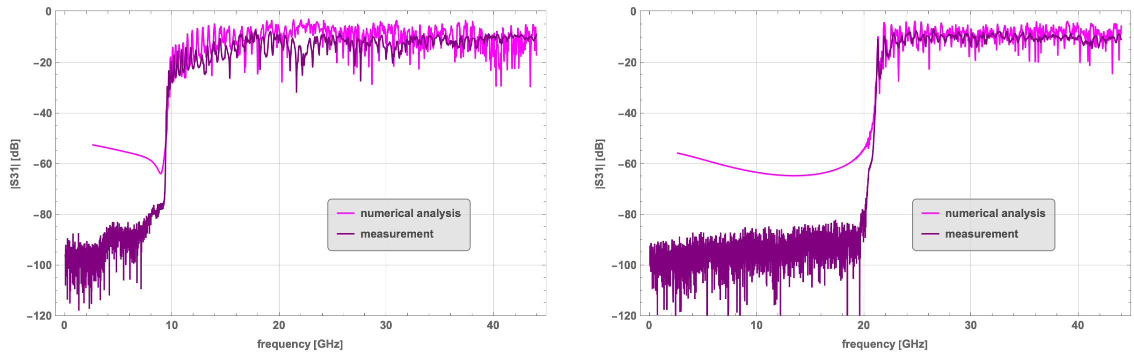

(a) For the coaxial adapter. (b) For the WR28 WG-to-coax adapter.

Figure 6: $|S31|(f)$ transfer function of the ChDR BPM target slab-line setup.

3. RF Measurements of a ChDR BPM pickup target

Figure 5 illustrates the slab-line setup, now extended with a 60 mm long ChDR BPM button pickup target mounted on the upper ground plane. Due to the ChDR surface area exposed to the slab-line center conductor a local increase of the characteristic impedance Z_{SL} is unavoidable, in the measurement it peaks to $\sim 62\,\Omega$ and in the simulation to $\sim 64\,\Omega$, as shown by the black, respectively red dashed trace in Fig. 4. We studied two different coaxial transmission-line transitions to measure the DR at the end of the circular, dielectric-loaded ChDR radiator waveguide: a simplistic coaxial adapter (Fig. 5a) and a *HP* type R281A waveguide-to-coaxial adapter (Fig. 5b), which results in an abrupt transition from the circular ChDR waveguide to a rectangular WR28 industry-standard waveguide. Both coaxial adapters suffer from a large mismatch of the TE11-mode wave impedance at the output surface of the circular ChDR waveguide, causing substantial scattering effects with multiple reflections in the setup. This leads to a rather "fractured" response of the $S31$ transfer function, see also Fig. 6, still with an acceptable agreement between the VNA measurement and the *CST* simulation. But, the latter shows larger scattering effects in the numerical $|S31|(f)$ data, probably in parts due to lower losses at high frequencies in the simulation. While the simple coaxial adapter (Fig. 6a) allows the characterization of the entire frequency range, including the TE11-mode cut-off frequency of the ChDR circular waveguide, $f_{TE11} \approx 9.3\,\text{GHz}$, the WR28 rectangular waveguide (Fig. 6b) suppresses the signal transmission below its TE01-mode cut-off frequency $f_{TE01} \approx 21.1\,\text{GHz}$

Figure 7 shows the time-domain (TD) impulse response waveform of the frequency-domain

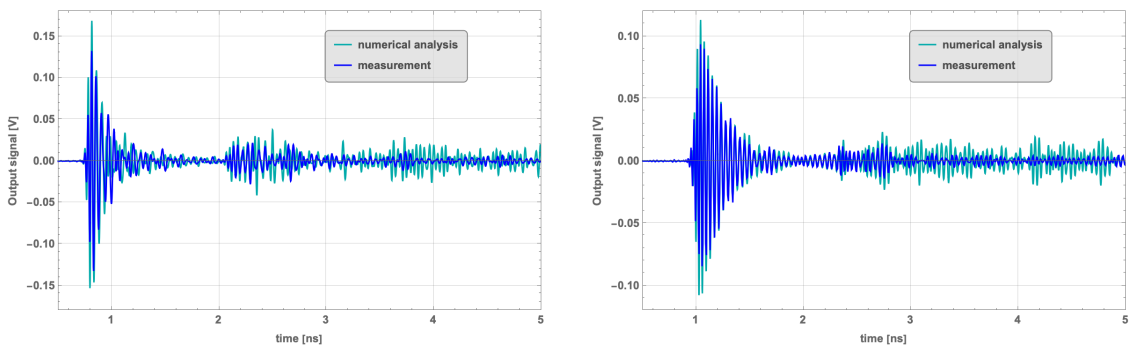

(a) For the coaxial adapter. (b) For the WR28 WG-to-coax adapter.

Figure 7: $S31$ time-domain impulse response of the ChDR BPM target slab-line setup.

Journal of Physics: Conference Series **2687** (2024) 072010 doi:10.1088/1742-6596/2687/7/072010

$S31$ measurement (blue traces) for the above examples, with the iFFT performed automatically inside the USB VNA. For comparison, the waveform of the *CST* simulation is shown in cyan color, and as expected from the $|S31|(f)$ data, the numerical TD response shows more “ringing” then the measured TD response.

4. Conclusions

The slab-line was used to characterise an alumina radiator in the lab for use in a ChDR BPM. The frequency and respective time response was obtained through measurements and compared to numerical analyses in *CST Studio*. These showed a reasonable level of agreement with discrepancies mainly caused by mechanical tolerances. More studies on the ChDR BPM are in progress, and the slab-line proves a valuable tool in aiding the development process of such a technology.

References

[1] Adli E, et al., Acceleration of electrons in the plasma wakefield of a proton bunch, *Nature* **561** 7723, pp. 363–367, Aug. 29, 2018. `doi: 10.1038/s41586-018-0485-4`

[2] Lefèvre T, et al., Cherenkov diffraction radiation as a tool for beam diagnostics, *Proc. IBIC'19*, Malmö, Sweden, Sep. 2019, pp. 660–664. `doi:10.18429/JACoW-IBIC2019-THAO01`

[3] Pakuza C, et al., A beam position monitor for electron bunch detection in the presence of a more intense proton bunch for the AWAKE experiment, *Proc. IPAC'22*, Bangkok, Thailand, Jun. 2022, pp. 381–384. `doi:10.18429/JACoW-IPAC2022-MOPOPT053`

[4] Pakuza C, et al., Electron beam studies on a beam position monitor based on Cherenkov diffraction radiation, *Proc. IPAC'23*, Venice, Italy, May 2023, paper THPL146 (*Preprint*).

[5] Chisholm R M, The characteristic impedance of trough and slab lines, *IEEE Transactions on Microwave Theory and Techniques* **4** 3, pp. 166–172, Jul. 1956. `doi:10.1109/tmtt.1956.1125045`